CORRELATION OF FIN BUFFET PRESSURES ON AN F/A-18
WITH SCALED WIND-TUNNEL MEASUREMENTS

Robert W. Moses
Aeroelasticity Branch
NASA Langley Research Center
Hampton, VA

Gautam H. Shah
Vehicle Dynamics Branch
NASA Langley Research Center
Hampton, VA

Abstract

Buffeting is an aeroelastic phenomenon occurring at high angles of attack that plagues high performance aircraft, especially those with twin vertical tails. Previous wind-tunnel and flight tests were conducted to characterize the buffet loads on the vertical tails by measuring surface pressures, bending moments, and accelerations. Following these tests, buffeting responses were computed using the measured buffet pressures and compared to the measured buffeting responses. The calculated results did not match the measured data because the assumed spatial correlation of the buffet pressures was not correct. A better understanding of the partial (spatial) correlation of the differential buffet pressures on the tail was necessary to improve the buffeting predictions. Several wind-tunnel investigations were conducted for this purpose. When compared, the results of these tests show that the partial correlation scales with flight conditions. One of the remaining questions is whether the wind-tunnel data is consistent with flight data. Presented herein, cross-spectra and coherence functions calculated from pressures that were measured on the High Alpha Research Vehicle (HARV) indicate that the partial correlation of the buffet pressures in flight agrees with the partial correlation observed in the wind tunnel.

Background

For high performance aircraft at high angles of attack, vortices emanating from wing/fuselage leading edge extensions (LEX) burst at some flight conditions, immersing the vertical tails in their wake, as shown in Figure 1 for the F/A-18. The resulting buffeting of the vertical tails are a concern from airframe fatigue and maintenance points of view. A summary of previous wind-tunnel[1-8] and flight tests [2, 5, 13] conducted to quantify fin buffet on the F/A-18 follows.

Figure 1. Flow Visualization of Leading Edge Extension (LEX) Vortex Burst, 30 Degrees Angle of Attack

Industry Test

The spectral nature of the unsteady differential (inboard surface minus outboard surface) pressures on the F/A-18 vertical tail caused by a burst LEX vortex are well documented[1]. As illustrated in Reference 1, the power spectral densities and root mean square (rms) values of the differential pressures vary with flight speed, angle of attack (AOA), dynamic pressure, and tail position. The worst case buffet condition, defined by the highest rms values of differential pressure at design limit load, occurs on the F/A-18 aircraft at a dynamic pressure of 340 pounds per square foot (psf) and 32 degrees angle of attack. Other findings of Reference 1 were that the rms value of the differential pressure varies linearly with dynamic pressure, and that Strouhal (proportional to reduced frequency) scaling provides a means for

comparing model and flight spectral data. Also, the highest rms values of differential pressure occur at stations closest to the leading edge while the lowest rms values occur near the trailing edge with a gradual change in rms values between these two regions of the tail. Another conclusion from this investigation was that the unsteady differential pressures were considered fully correlated (spatially in phase) since the pressures measured at five stations did not indicate a significant phase shift.
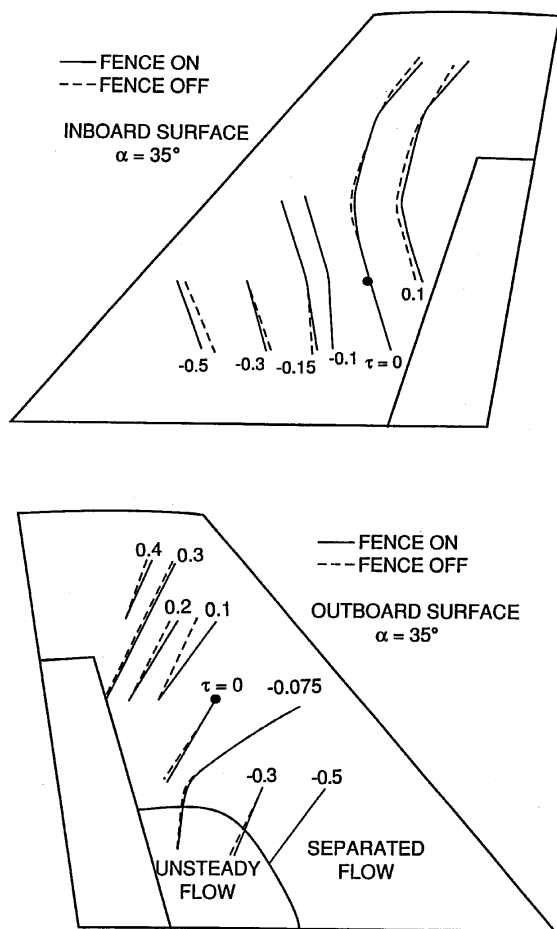
Canadian Measurements

Figure 2. Peak Correlation Contours (msec) of the Fin Unsteady Pressure Signals, Starboard-Side Rigid Tail, 6% F/A-18 Model, M=0.6, 35 Degrees AOA
(From Reference 2)

After the research of Reference 1, wind-tunnel tests of a 6% rigid F/A-18 model were conducted to investigate the spatial characteristics of the unsteady surface pressures on the tail[2]. Contour plots of the time delays of the unsteady pressures on each surface at Mach 0.6 were constructed using cross-correlation analyses of the measured unsteady pressures. As shown in Figure 2 for the two surfaces of the starboard-side fin, the contours above mid-span for inboard and outboard surfaces are quite different. It is in this region that the differential pressures contribute most to buffeting due to their distance from the root attachment at the fuselage. Therefore, the spatial characteristics of the unsteady differential pressures that contribute most to buffeting are unclear.
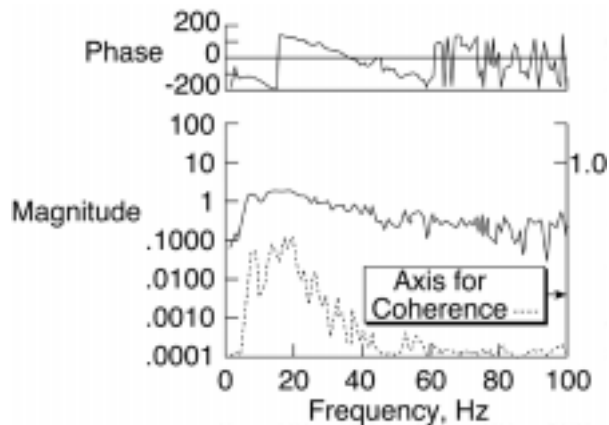
Prior Buffeting Predictions

Because of the perceived complexity in transcribing partially-correlated unsteady pressures into the analyses of buffet and buffeting, the differential pressures on the tail have been assumed to be in phase (fully correlated) at any given time[3-5]. These analyses do not estimate the buffet loads accurately, and it was concluded that an understanding of the spatial correlation of the pressures is a key to successful buffet load prediction and should be the subject of more research.
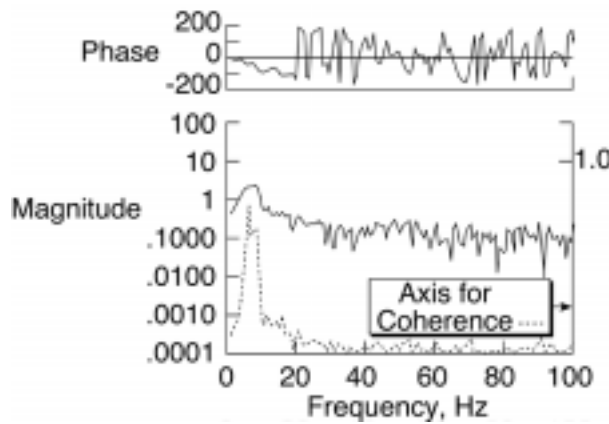
Full-Scale Wind-Tunnel Test

To learn more about the spatial correlation, a full-scale F/A-18 was tested in a wind tunnel[6-9] at high angles of attack at a maximum speed of M=0.15. Plots of the magnitudes and phase delays of the unsteady differential pressures at two stream-wise stations were constructed using cross-spectral analyses of the unsteady pressures measured on each tail surface at two different angles of attack (20 degrees and 32 degrees). The results shown in Figure 3a and 3b represent, respectively, harmless and worst case buffet conditions for the F/A-18. As shown in the Figures, the phase steadily decreases with increasing frequency. This trend is consistent for both angles of attack and indicates that the differential pressures acting on the tail are not in phase and therefore are not fully correlated. However, the relationship of flight conditions on

pressure correlation was not clearly understood from these results. Therefore, scaled model tests [8, 10-12] were conducted in the Transonic Dynamics Tunnel (TDT) where this relationship was determined, as summarized below.

The purpose of this paper is to evaluate whether the spatial correlation of the buffet pressures on an F/A-18 fin in flight agrees with the spatial correlation observed on a 1/6-scale F/A-18 fin in the TDT.

a) 20 Degrees AOA

b) 32 Degrees AOA

Figure 3. Cross-Spectral Density and Coherence Functions Between the Differential Pressures Near the Leading-Edge Tip and the Trailing-Edge Tip, Full-Scale Tail, M=0.15, (From Reference 6)

Scaled Wind-Tunnel Measurements

Figure 4. 1/6-Scale F/A-18 Model Mounted in the Transonic Dynamics Tunnel
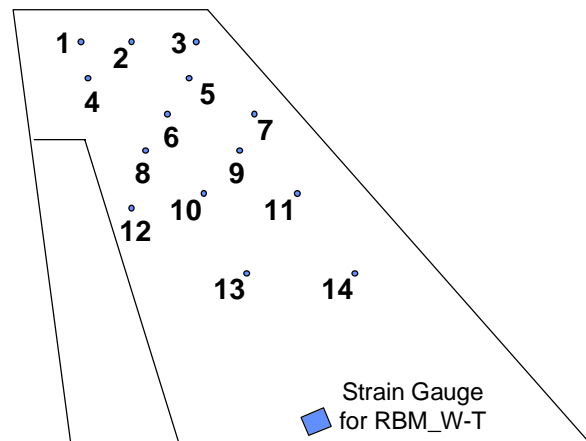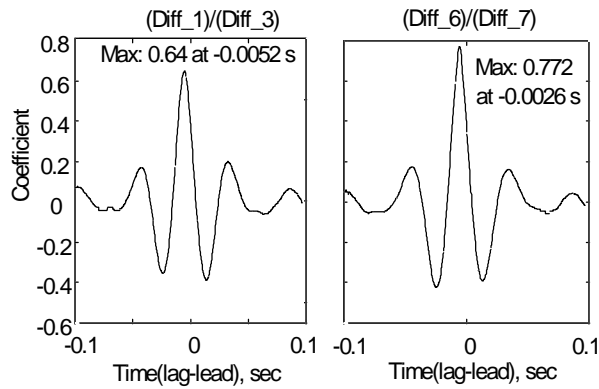

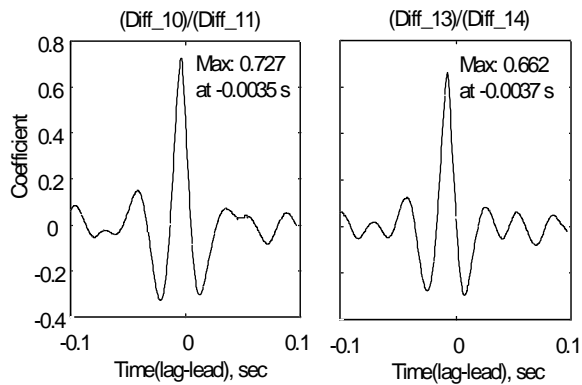Figure 5. Pressure Transducer Stations, 1/6-Scale Flexible Tail

To better understand the pressure correlation during buffet, an available 1/6-scale, sting-mounted, F-18 wind-tunnel model, shown in Figure 4, was modified and tested in the Transonic Dynamics Tunnel (TDT) at the NASA Langley Research Center as part of the ACROBAT (Actively Controlled Response Of Buffet-Affected Tails) program[8]. Surface pressures were measured for scaled flight conditions at high angles of attack on rigid and flexible tails. Using the transducer spread shown in Figure 5, cross-correlation and cross-spectral analyses[9] were performed for

identifying any consistent spatial characteristics of the unsteady differential pressures.

Cross-correlation and cross-spectral density (CSD) functions of the unsteady differential pressures on the flexible tail are shown in Figures 6 and 7, respectively, and compared to results of References 2 and 6, shown in Figures 2 and 3, respectively [10-12]. These comparisons show that the time and phase delays of the unsteady differential pressures scale with wind-tunnel speed. In fact, the unsteady differential pressures were found to resemble waves that move along the tail, as indicated by the non-zero time delays. So, one remaining question was the correlation of the wind-tunnel data with flight measurements.
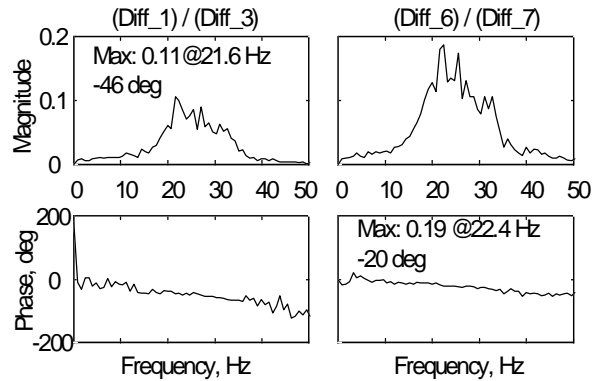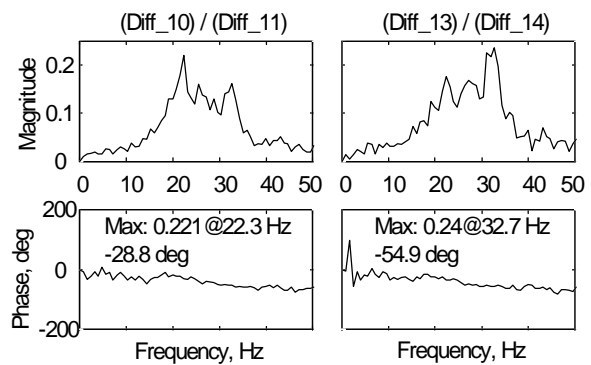

a) Near Tip and 75% Span

b) Near 60% and 40% Span

Figure 6. Cross-Correlation Functions Between Differential Pressures at Stations on Flexible Tail, 1/6-Scale F/A-18 Model, 34 Degrees AOA

a) Near Tip and 75% Span

b) Near 60% and 40% Span

Figure 7. CSD Functions Between Differential Pressures at Stations on Flexible Tail, 1/6-Scale F/A-18 Model, 34 Degrees AOA

Flight Test Results

Pressures on the surfaces of the starboard vertical tail of the HARV, shown in Figure 1, were measured at various flight conditions using a sampling rate of 320 Hz. Referring to the HARV fin shown in Figure 8, the even numbers represent pressure transducers on the shown surface (notation KS) while the odd numbers represent transducers on the hidden surface (notation KP). Therefore, the differential pressure computed for the station located at 85% span and 90% chord would be designated "KP31-KS32". This notation is used consistently herein for reporting the differential pressures on the HARV fin.

CSD functions of the unsteady differential pressures at Mach 0.3 and 30 degrees angle of attack were computed from the digitized time histories of 43 seconds in length using a block size of 2048 with 75% overlapping and a rectangular window.
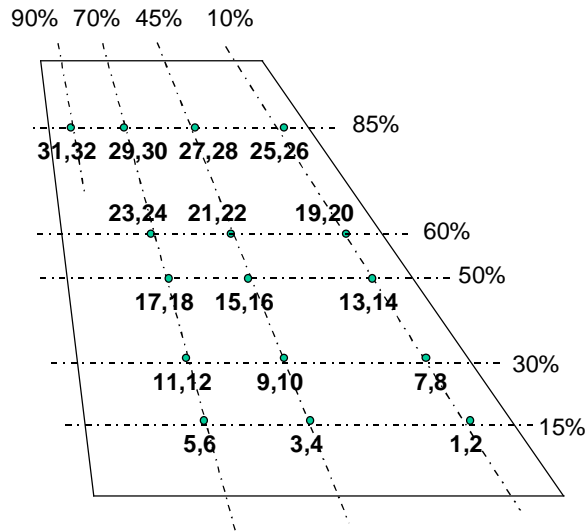

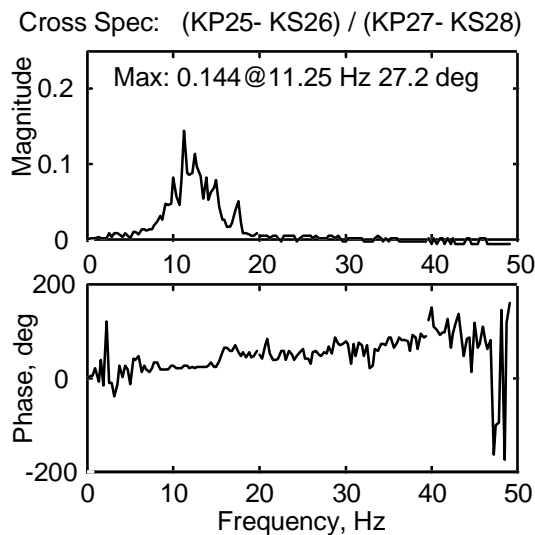Figure 8. Location of Pressure Transducer on Starboard Vertical Tail, HARV

Figure 9a. CSD Function Between Differential Pressures, Station KP25-KS26 with Respect to KP27-KS28, on HARV, Mach 0.3, 30 Degrees AOA, LEX Fence Off
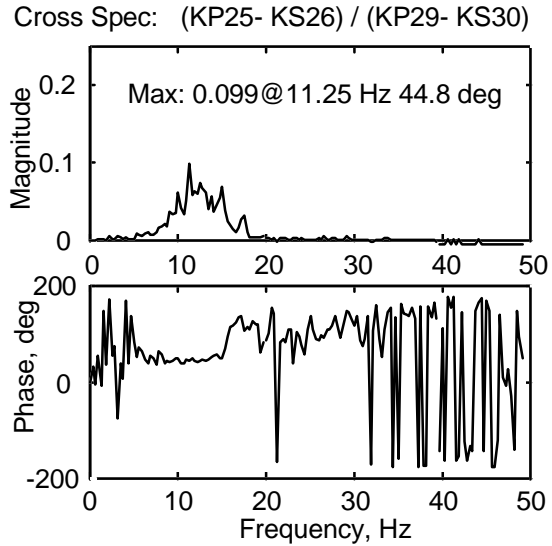

Figure 9b. CSD Function Between Differential Pressures, Station KP25-KS26 with Respect to KP29-KS30, on HARV, Mach 0.3, 30 Degrees AOA, LEX Fence Off

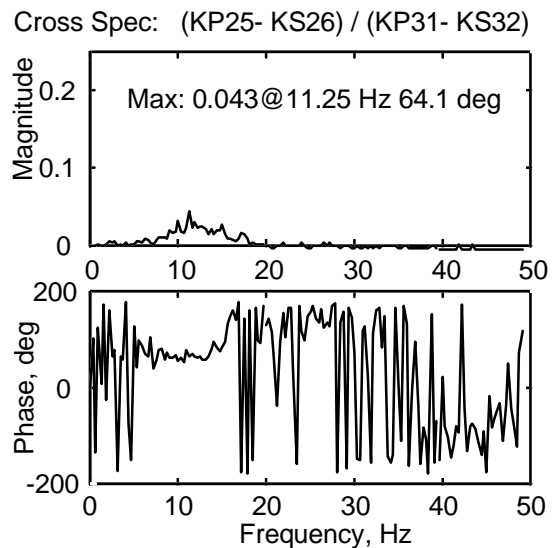Figure 9c. CSD Function Between Differential Pressures, Station KP25-KS26 with Respect to KP31-KS32, on HARV, Mach 0.3, 30 Degrees AOA, LEX Fence Off

The magnitude and phase of the CSD functions, plotted in Figure 9, illustrate the spatial features of the differential pressures along the 85% span line. Based on the location of the peak magnitude in the upper plots in Figures 9a, 9b and 9c, the dominant

frequency component of the buffet pressures at these locations is approximately 11.25 Hz. In fact, the overall shape of the curve shown in all three magnitude plots are quite similar except for the relative scale in the vertical direction. The magnitudes of the CSD functions decrease with increase in distance between stations moving aft. This effect is expected since the rms of the differential pressures is generally highest at the stations near the leading edge and generally lowest near the stations near the trailing edge.

The value of phase between stations is conversely affected by distance. As shown in Figure 9, the value of the phase at the dominant frequency of 11.25 Hz is different in each of the lower plots. For instance, in Figure 9a, the phase at 11.25 Hz is approximately 27 degrees while, in Figure 9b, the phase is approximately 45 degrees, and while in Figure 9c, the phase is approximately 64 degrees. With reference to the 85% span-line in Figure 8, the pressure wave, represented by the CSD in Figure 9a, traveled 35% of the chord while the pressure wave, represented by the CSD in Figure 9b, traveled 60% of the chord length. Therefore, the phase increases with increases in distance between stations. Furthermore, this relationship appears to be linear.

As a check of linearity, the phase, shown in Figure 9a, is computed for the pair of differential pressure transducers KP25-KS26 and KP27-KS28 which are 1.54 feet apart. At 30 degrees AOA, the velocity of the streamlines in the vicinity of the tail will be less than the flight speed of Mach 0.3 (330 feet per second). In Reference 12, the velocity near the tail is shown to be approximately 70% of the free stream value. Therefore, using Equation 1, where "f" is the frequency of interest (11.25 Hz in this case), "d" is the distance between stations, and "U" is the velocity of the streamline near the 85% span line, the phase at 11.25 Hz is computed as 27 degrees, which agrees well with the value shown in Figure 9a. Similarly, the phase may be computed for other pressure transducer pairs. Equation 1 may be simplified further by introducing the Strouhal number, defined by Equation 2, and canceling like terms, to yield Equation 3.

$$\phi(\mathrm{rad}) = \omega \cdot t = 2\pi \mathrm{f} \cdot \frac{\mathrm{d}}{\mathrm{U}} \qquad (1)$$

$$\mathrm{n} = \frac{\mathrm{f\,d}}{\mathrm{U}} \qquad (2)$$

$$\phi\,(\mathrm{deg}) = \phi\,(\mathrm{rad}) \cdot \frac{180}{\pi} = 360\,\mathrm{n} \qquad (3)$$

Since dispersion (break down of eddies into higher harmonics) and dissipation (energy loss) are expected in this highly turbulent flow near the tail, the pressure wave is expected to deform as it travels along the tail[12]. Therefore, the magnitude of the partial correlation of the differential pressures at two stations is expected to drop as the distance between these two pressure stations increases. The coherence function provides a tool for assessing this drop in correlation. In Figure 10, coherence functions are computed, with respect to KP25-KS26, for the differential pressures at selected stations along the 85% span line for Mach 0.3, 30 degrees AOA.
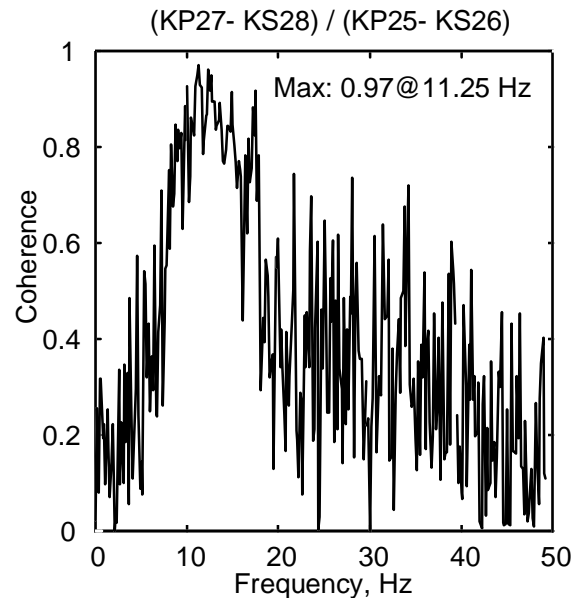

Figure 10a. Coherence Function Between Differential Pressures on HARV, Along 85% Span Line, Station KP27-KS28 with Respect to KP25-KS26, Mach 0.3, 30 Degrees AOA, LEX Fence Off

(KP29- KS30) / (KP25- KS26)
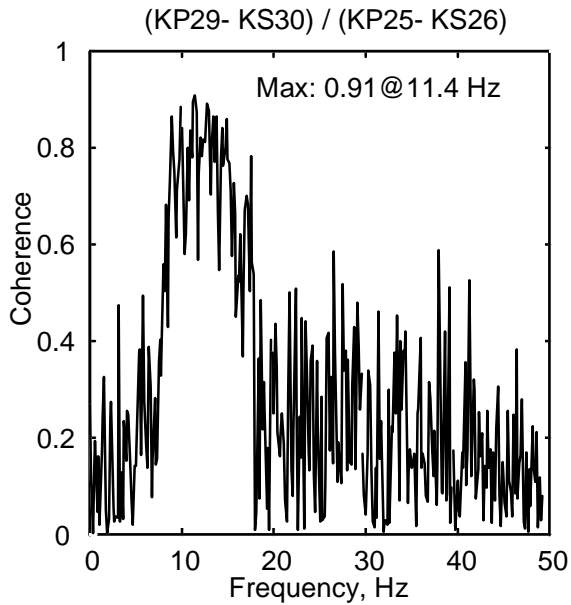
Max: 0.91@11.4 Hz

Coherence vs Frequency, Hz

Figure 10b. Coherence Function Between
Differential Pressures on HARV,
Along 85% Span Line,
Station KP29-KS30 with Respect to KP25-KS26,
Mach 0.3, 30 Degrees AOA, LEX Fence Off

(KP19- KS20) / (KP25- KS26)

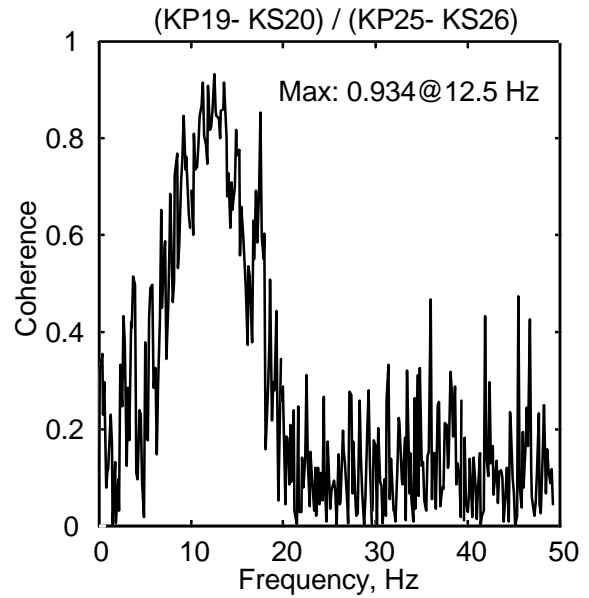Max: 0.934@12.5 Hz

Coherence vs Frequency, Hz

Figure 11a. Coherence Function Between
Differential Pressures on HARV,
Along 10% Chord Line,
Station KP19-KS20 with Respect to KP25-KS26,
Mach 0.3, 30 Degrees AOA, LEX Fence Off

(KP31- KS32) / (KP25- KS26)

Max: 0.79@10.9 Hz
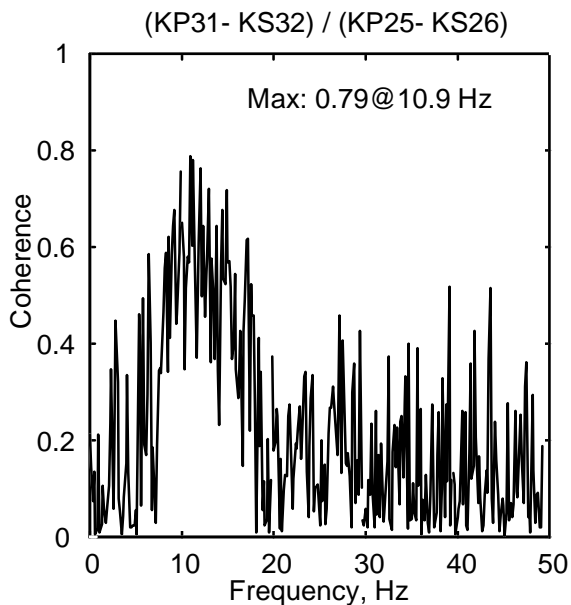
Coherence vs Frequency, Hz

Figure 10c. Coherence Function Between
Differential Pressures on HARV,
Along 85% Span Line,
Station KP31-KS32 with Respect to KP25-KS26,
Mach 0.3, 30 Degrees AOA, LEX Fence Off

(KP13- KS14) / (KP25- KS26)

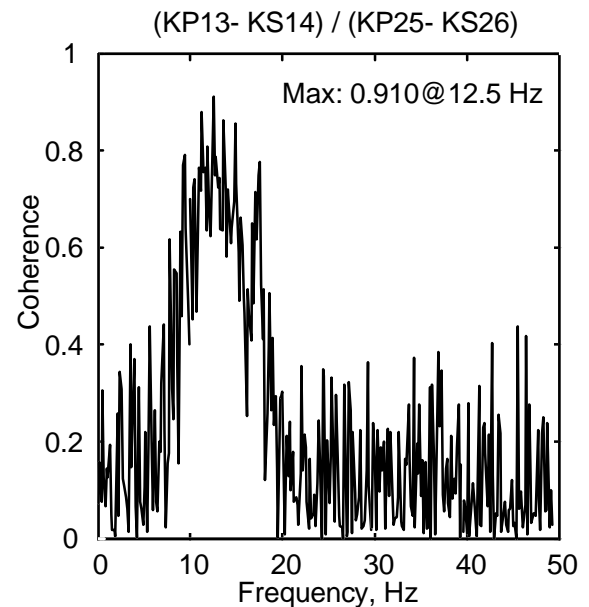Max: 0.910@12.5 Hz

Coherence vs Frequency, Hz

Figure 11b. Coherence Function Between
Differential Pressures on HARV,
Along 10% Chord Line,
Station KP13-KS14 with Respect to KP25-KS26,
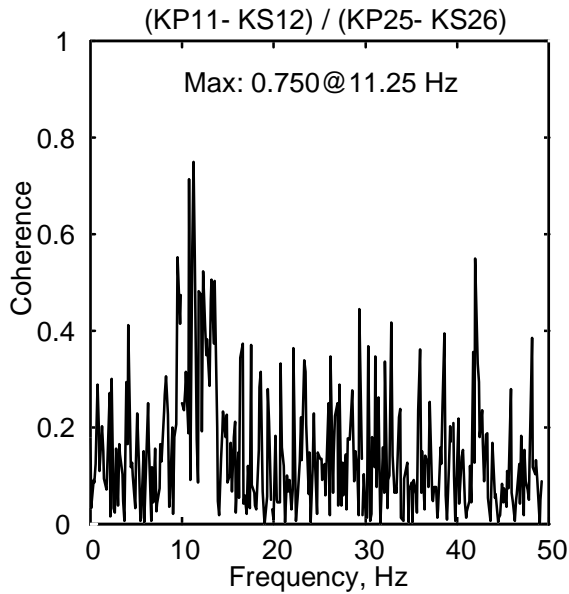Mach 0.3, 30 Degrees AOA, LEX Fence Off

Figure 12. Coherence Function Between
Differential Pressures on HARV,
Well Separated Stations,
Station KP11-KS12 with Respect to KP25-KS26,
Mach 0.3, 30 Degrees AOA, LEX Fence Off

In Figure 10a, the maximum value of the coherence is 0.97 (out of a possible 1.0) at 11.25 Hz, the dominant frequency in the pressure wave form. The values of the coherence for other frequency components in the pressure wave are less than 0.97. This feature indicates that some dispersion of the frequency components is occurring as the wave moves along the tail. For instance, if the values of the coherence for all frequency components are unity, then no dispersion occurs in the wave as it moves along the tail. Conversely, if the values of the coherence for all frequency components get smaller as the distance between stations increases, then all frequency components in the wave are dispersing as a function of distance. The latter case is the nature of the unsteady differential pressures that occur on the vertical tails during buffet caused by LEX vortex burst.

As the pressure wave moves aft along the 85% span line, the maximum value in the coherence function falls from 0.97, shown in Figure 10a, to 0.91, shown in Figure 10b, to 0.79, shown in

Figure 10c. Therefore, some dispersion and possibly some dissipation are occurring along a chord line. For the 10% chord line, the maximum value in the coherence functions are 0.934, shown in Figure 11a, and 0.91, shown in Figure 11b. Therefore, more dispersion occurs along a constant span line than along a constant chord line. The smallest maximum values of the coherence functions occur for stations that are farthest apart, as seen in Figure 12, where the maximum value is 0.75. Therefore, the worst coherence occurs between the most separated stations.

Comparison of Flight Results With
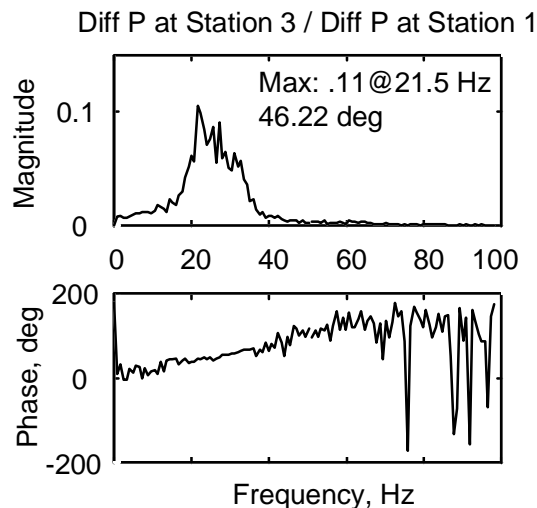Scaled Wind-Tunnel Results

Figure 13. Cross-Spectral Density Function
Between Differential Pressures,
1/6-Scale F/A-18 Model,
Along Constant Span Line,
Station 3 with Respect to Station 1,
Mach 0.6 (Simulated), 34 Degrees AOA

Based on Strouhal scaling, the CSD functions, shown in Figure 7, that were computed for pressures measured in the TDT on a 1/6-scale F/A-18 vertical tail at Mach 0.1 (110 feet per second) at 34 degrees AOA, are representative of an F/A-18 at Mach 0.6 (660 feet per second) at 34 degrees AOA. Shown in Equation 1, a doubling of flight speed will reduce the phase shift by 50%, and from Reference 1, a doubling of the flight

speed will also double the frequency value at which the peak magnitude of the CSD occurs. This latter effect can be seen also in Equation 2 when maintaining a constant value of n. Therefore, since the two effects cancel each other in this case, a direct comparison of the phase value at the peak magnitude of the CSD function is possible between wind-tunnel results for the 1/6-scale F/A-18 model and the results of the HARV at Mach 0.3.
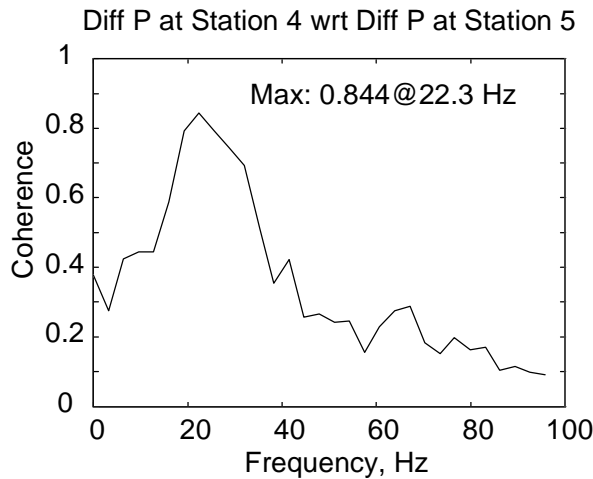
Diff P at Station 4 wrt Diff P at Station 5

Max: 0.844@22.3 Hz

Figure 14. Coherence Function Between
Differential Pressures,
1/6-Scale F/A-18 Model,
Station 4 with Respect to Station 5,
Mach 0.6 (Simulated), 34 Degrees AOA

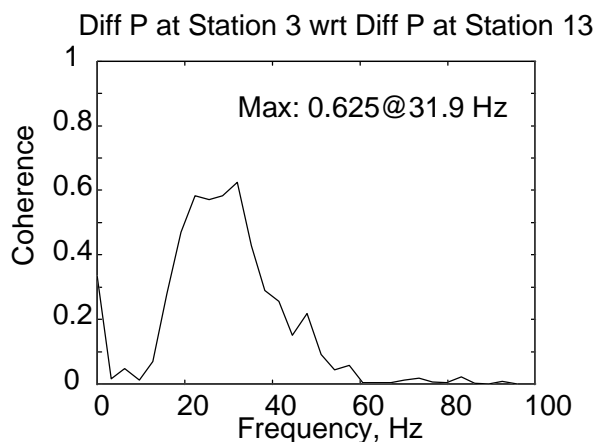Diff P at Station 3 wrt Diff P at Station 13

Max: 0.625@31.9 Hz

Figure 15. Coherence Function Between
Differential Pressures,
1/6-Scale F/A-18 Model,
Station 3 with Respect to Station 13,
Mach 0.6 (Simulated), 34 Degrees AOA

In Figure 13, the CSD plot shows that the phase between the differential pressure at Station 3 with respect to Station 1 on the 1/6-scale F/A-18 vertical tail at 34 degrees AOA is approximately 46 degrees. For similar conditions and stations on the HARV, the phase is approximately 45 degrees, as shown in Figure 9b.

Coherence functions were computed for selected stations on the 1/6-scale F/A-18 flexible vertical tail for comparing coherence functions computed for the HARV.   Shown in Figure 14, the maximum value of the coherence function between stations 4 and 5 on the 1/6-scale F/A-18 vertical tail (see Figure 5) is 0.844. This value of 0.844 agrees well with the values of the coherence functions, shown in Figures 10b (0.91) and 10c (0.79), for similar stations on the HARV vertical tail (see Figure 8). For an additional comparison, the coherence function between two of the most separated stations on the 1/6-scale F/A-18 flexible vertical tail was computed, as shown in Figure 15. The maximum value of the coherence between stations 3 and 13 on the 1/6-scale F/A-18 vertical tail (see Figure 5) is 0.625. This value is less than but not too different from the maximum value of 0.75 for the coherence function, shown in Figure 12, between stations that are similarly separated in terms of percent chord and percent span. Therefore, the level of dispersion occurring on the fins of the 1/6-scale model and the HARV agree well.

Conclusions

CSD and coherence functions were presented for indicating the partial (spatial) correlation that occurs on the vertical tail of the F/A-18 configuration during LEX vortex burst. The unsteady buffet pressures that are caused by LEX vortex burst during high angle of attack maneuvers on the F/A-18 (HARV) are not fully correlated as previously assumed. In fact, the local Strouhal number may be used to relate the phase shift of the unsteady buffet pressures among stations on the vertical tail.

The magnitude of the CSD functions presented herein indicates that the vortex disturbance

reduces as it travels along the tail. In agreement with this finding, the magnitudes of the coherence functions illustrate that the correlation of the unsteady pressures is affected by the distance between the stations. One issue that surfaces from this finding is the role, if any, that the vertical tail plays in affecting the spatial correlation and dispersion of the unsteady buffet pressures.

As shown herein, the results presented for the HARV agree well with the partial correlation of the buffet differential pressures measured on a 1/6-scale F/A-18 model tested in the TDT. Comparisons between the 1/6-scale F/A-18 data and the F/A-18 (HARV) data consistently illustrate the partial correlation of the differential pressures that occur on the vertical tail during LEX vortex burst at high angles of attack.

Acknowledgments

References

1 Zimmerman, N. H., and Ferman, M. A., "Prediction of Tail Buffet Loads for Design Application," Vols. I and II, Rept. No. NADC-88043-60, July 1987.

2 Lee, B., Brown, D., Zgela, M., and Poirel, D., "Wind Tunnel Investigation and Flight Tests of Tail Buffet on the CF-18 Aircraft", in Aircraft Dynamic Loads Due to Flow Separation, AGARD-CP-483, NATO Advisory Group for Aerospace Research and Development, Sorrento, Italy, April 1990.

3 Lee, B. and Tang, F. C., "Unsteady Pressure and Load Measurements on an F/A-18 Vertical Fin at High-Angles-of-Attack," AIAA-92-2675-CP, 10th Applied Aerodynamics Conference, Palo Alto, CA, June 22-24, 1992.

4 James, K. D. and Meyn, L. A., "Dependence on Integrated Vertical-Tail Buffet Loads for F/A-18 on Sensor Density," SAE Technical Paper 94110, Aerospace Atlantic Conference and Exposition, Dayton, Ohio, April 18-22, 1994.

5 Bean, D. E. and Lee, B., "Correlation of Wind Tunnel and Flight Test Data for F/A-18 Vertical Tail Buffet," AIAA-94-1800-CP, 12th AIAA Applied Aerodynamics Conference, Colorado Springs, CO, June 20-22, 1994.

6 Pettit, C. L., Banford, M., Brown, D., and Pendleton, E., "Pressure Measurements on an F/A-18 Twin Vertical Tail in Buffeting Flow," Vols 1-4, United States Air Force Wright Laboratory, TM-94-3039, August 1994.

7 Meyn, L. A. and James, K. D., "Full-Scale Wind-Tunnel Studies of F/A-18 Tail Buffet," Journal of Aircraft, Vol. 33, No. 3, May-June 1996.

8 Moses, R. W., "Active Vertical Tail Buffeting Alleviation on a Twin-Tail Fighter Configuration in a Wind Tunnel," presented at the CEAS International Forum on Aeroelasticity and Structural Dynamics 1997, 17-20 June 1997, Rome, Italy.

9 Bendat, J. S. and Piersol, A. G., Engineering Applications of Correlation and Spectral Analysis, Second Edition, John Wiley & Sons, Inc., 1993.

10 Moses, R. W. and Pendleton, E., "A Comparison of Pressure Measurements Between a Full-Scale and a 1/6-Scale F/A-18 Twin Tail During Buffet," AGARD Report 815, p. 6-1 to p. 6-12, Florence, Italy, September 4-5, 1996.

11 Moses, R. W. and Ashley, H., "Spatial Characteristics of the Unsteady Differential Pressures on 16% F/A-18 Vertical Tails," AIAA 98-0519, 36th AIAA Aerospace Sciences Meeting and Exhibit, Reno, Nevada, January 12-15, 1998.

12 Moses, Robert W., "Spatial Characteristics of the Unsteady Differential Pressures on Vertical Tails of a Twin-Tailed Aircraft at High Angles of Attack with an Emphasis on Buffeting Alleviation," Ph.D. Dissertation, Stanford University, August 1997.

13 Moses, R. and Shah, G., "Spatial Characteristics of F/A-18 Vertical Tail Buffet

Pressures Measured in Flight," AIAA-98-1956, 39th AIAA/ASME/ASCE/AHS/ASC Structures, Structural Dynamics, and Materials Conference and Exhibit, Long Beach, CA, 20-23 April 1998.